AD-A227 904

REPORT DOCUMENTATION PAGE

Form Approved
OMB No. 0704-0188

1. AGENCY USE ONLY (Leave blank)	2. REPORT DATE	3 REPORT TYPE AND DATES COVERED
	8 Jul 86	Conference Presentation

4. TITLE AND SUBTITLE
Control of Wake Structure Behind an Oscillating Airfoil

5. FUNDING NUMBERS
TA 2307-F1-38

6. AUTHOR(S)
M.C. Robinson, H.E. Helin, M.W. Luttges

7. PERFORMING ORGANIZATION NAME(S) AND ADDRESS(ES)
F.J. Seiler Research Laboratory
USAF Academy CO 80840-6528

8. PERFORMING ORGANIZATION REPORT NUMBER
FJSRL-PR-90-0004

9. SPONSORING / MONITORING AGENCY NAME(S) AND ADDRESS(ES)

10. SPONSORING / MONITORING AGENCY REPORT NUMBER

11. SUPPLEMENTARY NOTES

12a. DISTRIBUTION / AVAILABILITY STATEMENT
Distribution Unlimited

12b. DISTRIBUTION CODE

13. ABSTRACT (Maximum 200 words)

The initiation, development, and shedding of vortices induced by sinusoidal airfoil motions were examined in the airfoil wake across a range of independent forcing parameters. Then, the interactions of these wakes with a following or trailing airfoil were studied. Coherent, phase-dependent, tandem vortex wake structures emerged from the shedding vorticity of the upstream oscillating airfoi. Consistent interactions of the vortex wake with a trailing airfoil were revealed with both the multiple-exposure, phase-locked, flow visualization measures and the time-dependent surface pressure measurements. Impingement of the tandem vortex wake upon the trailing airfoil produced unsteady pressure distributions resulting in very transient loading. Similar effects in unsteady loading were observed when an auto-rotating flat plate was used to create a vortex-dominated wake. These findings suggest that a consistent, structured wake produced by unsteady separation might be used to produce desired lift characteristics on a trailing, lifting surface.

14. SUBJECT TERMS
flow visualization,
dynamic loads
vortices. (JND) E

15. NUMBER OF PAGES
15

16. PRICE CODE

17 SECURITY CLASSIFICATION OF REPORT	18 SECURITY CLASSIFICATION OF THIS PAGE	19 SECURITY CLASSIFICATION OF ABSTRACT	20. LIMITATION OF ABSTRACT
UNCLASSIFIED	UNCLASSIFIED	UNCLASSIFIED	NONE

GENERAL INSTRUCTIONS FOR COMPLETING SF 298

The Report Documentation Page (RDP) is used in announcing and cataloging reports. It is important that this information be consistent with the rest of the report, particularly the cover and title page. Instructions for filling in each block of the form follow. It is important to ***stay within the lines*** to meet ***optical scanning requirements.***

Block 1. Agency Use Only *(Leave blank)*

Block 2. Report Date Full publication date including day, month, and year, if available (e.g. 1 Jan 88). Must cite at least the year.

Block 3. Type of Report and Dates Covered. State whether report is interim, final, etc. If applicable, enter inclusive report dates (e.g. 10 Jun 87 - 30 Jun 88).

Block 4. Title and Subtitle. A title is taken from the part of the report that provides the most meaningful and complete information. When a report is prepared in more than one volume, repeat the primary title, add volume number, and include subtitle for the specific volume. On classified documents enter the title classification in parentheses.

Block 5. Funding Numbers. To include contract and grant numbers; may include program element number(s), project number(s), task number(s), and work unit number(s). Use the following labels:

C	- Contract	PR	- Project
G	- Grant	TA	- Task
PE	- Program Element	WU	- Work Unit Accession No.

Block 6. Author(s) Name(s) of person(s) responsible for writing the report, performing the research, or credited with the content of the report. If editor or compiler, this should follow the name(s)

Block 7. Performing Organization Name(s) and Address(es) Self-explanatory

Block 8. Performing Organization Report Number Enter the unique alphanumeric report number(s) assigned by the organization performing the report

Block 9. Sponsoring/Monitoring Agency Name(s) and Address(es) Self-explanatory

Block 10. Sponsoring/Monitoring Agency Report Number *(If known)*

Block 11. Supplementary Notes Enter information not included elsewhere such as: Prepared in cooperation with ; Trans. of ; To be published in When a report is revised, include a statement whether the new report supersedes or supplements the older report

Block 12a. Distribution/Availability Statement. Denotes public availability or limitations. Cite any availability to the public. Enter additional limitations or special markings in all capitals (e.g. NOFORN, REL, ITAR).

- **DOD** - See DoDD 5230.24, "Distribution Statements on Technical Documents."
- **DOE** - See authorities.
- **NASA** - See Handbook NHB 2200.2.
- **NTIS** - Leave blank.

Block 12b. Distribution Code

- **DOD** - Leave blank.
- **DOE** - Enter DOE distribution categories from the Standard Distribution for Unclassified Scientific and Technical Reports.
- **NASA** - Leave blank.
- **NTIS** - Leave blank.

Block 13. Abstract Include a brief *(Maximum 200 words)* factual summary of the most significant information contained in the report.

Block 14. Subject Terms. Keywords or phrases identifying major subjects in the report

Block 15. Number of Pages Enter the total number of pages

Block 16. Price Code. Enter appropriate price code *(NTIS only)*

Blocks 17. - 19. Security Classifications Self-explanatory Enter U.S. Security Classification in accordance with U.S. Security Regulations (i.e., UNCLASSIFIED) If form contains classified information, stamp classification on the top and bottom of the page.

Block 20. Limitation of Abstract This block must be completed to assign a limitation to the abstract. Enter either UL (unlimited) or SAR (same as report) An entry in this block is necessary if the abstract is to be limited If blank, the abstract is assumed to be unlimited

CONTROL OF WAKE STRUCTURE BEHIND AN OSCILLATING AIRFOIL

M. C. Robinson,* H. E. Helin,** and M. W. Luttges***
Department of Aerospace Engineering Sciences
University of Colorado
Boulder, Colorado 80309-0429

Abstract

The initiation, development, and shedding of vortices induced by sinusoidal airfoil motions were examined in the airfoil wake across a range of independent forcing parameters. Then, the interactions of these wakes with a following or trailing airfoil were studied. Coherent, phase-dependent, tandem vortex wake structures emerged from the shedding vorticity of the upstream oscillating airfoil. Consistent interactions of the vortex wake with a trailing airfoil were revealed with both the multiple-exposure, phase-locked, flow visualization measures and the time-dependent surface pressure measurements. Impingement of the tandem vortex wake upon the trailing airfoil produced unsteady pressure distributions resulting in very transient loading. Similar effects in unsteady loading were observed when an auto-rotating flat plate was used to create a vortex-dominated wake. These findings suggest that a consistent, structured wake produced by unsteady separation might be used to produce desired lift characteristics on a trailing, lifting surface. To achieve this, wake impingement angles and trailing airfoil angles of attack interactions must be evaluated in more detail.

Nomenclature

c	airfoil chord
K	reduced frequency = $\omega c/2U_\infty$
Re	Reynolds number = $U_\infty c/\nu$
U_∞	freestream velocity
ν	kinematic viscosity
ω	rotational rate (rad/sec)
C_L	airfoil lift coefficient
C_p	airfoil pressure coefficient

Introduction

Unsteady aerodynamics and, in particular, vortex dominated flowfields have become an area of intense interest in recent years.[1,2,3] Initially, studies were motivated by efforts to reduce or avoid the undesirable loading effects flow fields.[4,5,6] However, numerous recent studies have focused on efforts to gain a better understanding of the means through which unsteady flows might be controlled. Unsteady flow generation techniques also have been studied as a means of enhancing aerodynamic performance. Enhanced lift and reduced separation has been demonstrated through vortex generation from oscillating airfoils,[7] pulsed air injection,[8] oscillating spoilers[9] and interrupted pitching motions.[10]

Nestled in these attempts to enhance aerodynamic performance through manipulation of unsteady separated flows are a variety of aerodynamic interactions with downstream lifting surfaces. Understanding how unsteady flows will interact with such surfaces will play an important role in the predictability and control of aerodynamic loading. Emerging and "testbed" aircraft such as the X-29 with a leading canard and trailing forward swept wing emphasize the importance of these kinds of flow interactions. In addition, supermaneuverability and post-stall performance such as that postulated by Herbst,[11] will require precise prediction and control of surface interactions with forced unsteady separated flows.

The phase relationships between the unsteady aerodynamics experienced by a downstream body from an upstream source are a complex function of both time and distance.[12] The interactions and resultant loading are problems inherently dependent on the forcing parameters which generate the unsteadiness.[13] Initial studies on unsteady boundary layers and impinging wakes on trailing airfoils have been both fruitful and enlightening.[12,14,15,16] These initial studies have been expanded to encompass separated large scale vortical wakes impinging on a trailing airfoil at zero incidence. Wake effects were investigated through phase locked flow visualization and instantaneous surface pressure measurements made on the trailing airfoil. The coupled effects of Reynolds number and reduced frequency of the forcing model were examined.

Methods

These studies were conducted in the 2 ft. x 2 ft. low speed wind tunnel at the University of Colorado. The primary model of a trailing airfoil was a full span 6" chord NACA 0015 airfoil. This airfoil was instrumented with 18 Endevco 8507-2 miniature pressure transducers close-coupled to the airfoil surface. Further information on the instrumentation and data acquisition processing is detailed elsewhere.[17] The instrumented airfoil was mounted statically at geometric zero incidence angle in the center of the wind tunnel test section. The leading

* Assistant Professor Adjunct, Department of Aerospace Engineering Sciences, Member AIAA
** Graduate Research Associate, Department of Aerospace Engineering Sciences, Member AIAA
*** Professor, Department of Aerospace Engineering Sciences, Member AIAA

edge of the airfoil was mounted 0.5 chord lengths behind an upstream pitching model. The upstream pitching model had two forms depending on test conditions. The first of these was a full span 6" chord NACA 0015 airfoil which could be pitched sinusoidally about a quarter chord axis. The mean angle of attack for this pitching airfoil was 15° and the amplitude of oscillation was $\pm$ 6°. The reduced frequencies were varied between 0.05 and 0.8. These airfoil motion parameters were selected through separate studies using a full span 6" chord flat plate. The unsteady vortex dynamics and resultant wake structures were examined as a function of the oscillation rate and mean angle of attack. The sinusoidally oscillated model forced a very asymmetrical, period-dependent wake which impacted on the trailing airfoil. The second dynamic model coupled with the trailing airfoil was an auto-rotating flat plate. The 3" chord, full span model was allowed to rotate on low friction needle bearings and generate a periodic, free developing wake.

The unsteady vortex-dominated wake effects on the trailing airfoil were examined both as a function of the dynamic upstream model motion parameters and as a function of Reynolds number. The Reynolds number based on the 6" chord trailing airfoil was varied between 50,000 and 200,000. The instantaneous surface pressures on the trailing airfoil were recorded over two full cycles of upstream model motion (four cycles in the 40 ft/s auto-rotating plate tests). During this period, each of the 18 pressure ports was sequentially sampled 200 times. The process was repeated 25 times to obtain an ensemble average. The data were reduced to provide instantaneous airfoil pressure coefficients (C_p) and integrated lift coefficients (C_L).

In addition to the surface pressure measurements, phase-locked stroboscopic flow visualization studies of the individual components and coupled component systems were conducted. A series of dense smoke streaklines were generated in the test section using Roscoe Fog Fluid. A low pressure delivery of smoke to an airfoil smokerake in the wind tunnel settling chamber provided flow marking. Multiple exposure, phase-locked photographs were obtained with an electronic trigger coupled to a 35mm SLR camera and high intensity (7 μsec duration) stroboscopic flash unit.

Results

Unsteady separated flow produced by sinusoidal oscillations of an airfoil beyond static stall was dominated by the passage of large vortical structures over the airfoil and into the wake. Variance in vortex size, shape and cohesiveness was observed as a function of the parameters governing the oscillation motion history of the airfoil. Many of the influences exerted by the vortex-dominated wake passing over the trailing airfoil were assessed using time-correlated flow visualization measures in conjunction with surface pressure measurements. Duplicate test conditions were used for both measurement methodologies. Airfoil pitching dynamics directly controlled the development of the wake structures as well as the effects of these wake structures on the trailing airfoil.

The general patterns of vortex structures elicited by an airfoil oscillating sinusoidally in pitch have been documented previously. A small vortex emerges from the separated flow at the airfoil leading edge usually during the upstroke portion of the oscillation cycle at angles of attack well beyond static stall angles. The presence of the dynamically-produced leading edge vortex reattaches what would have been fully separated flow in static angles of attack tests. Vortex initiation and development over the oscillating airfoil are especially dependent on test dynamics with the separation vortex exhibiting both varying rapid growth rates and a range of convection velocities. When the leading edge vortex sheds from the surface of the upstream airfoil, a second vortex of opposite circulation is often initiated about the trailing edge of this airfoil. In the wake, the leading and trailing edge vortices combined to form a tandem structure which remained coherent for several chord diameters into the wake.

Alterations in the development of tandem vortical wake structure were examined as a consequence of airfoil motion parameters: 1) mean angle of attack, 2) oscillation angle, 3) oscillation rate and Reynolds number. For select cases, the impingement pressures created by the tandem wake structures impacting upon a trailing airfoil also were investigated. For comparison purposes, the impingement of vortices produced by an auto rotating flat plate were tested using the pressure-instrumented airfoil.

Short duration, multiple exposure photographs were prepared using phase-specific parts of the oscillation cycle to document wake vortex reproducibility. In the analysis superimposed smokelines from successive phase-locked exposures revealed repeatable vortex characteristics whereas disparate or diffuse smoke patterns indicated oscillation-independent flows. This visualization analysis permitted a rapid assessment to be made of the wake flow characteristics across a range of test parameters.

Mean Angle Of Attack

The multiple (15 flashes) exposure visualizations of Fig. 1, show 1) the shedding of the leading edge vortex and subsequent initiation of the trailing edge vortex, 2) the growing wake interaction between the leading and trailing edge vortices and 3) the fully developed flow disturbance in the wake. Each of these three phases of shedding vortex interactions is depicted in the three columns. Plates A-E contrast the wake development for increasing mean angle of attack values of 10, 15, 20, 25, and 30°, respectively. The oscillation angle and oscillation rate were held constant across the test conditions (α_ω = 6°, K = 0.6).

In each frame of Fig. 1, the development and interaction of the vortices with the oscillating flat plate and with each other were clearly evident. The evolution of the trailing edge vortex as a consequence of mean angle of

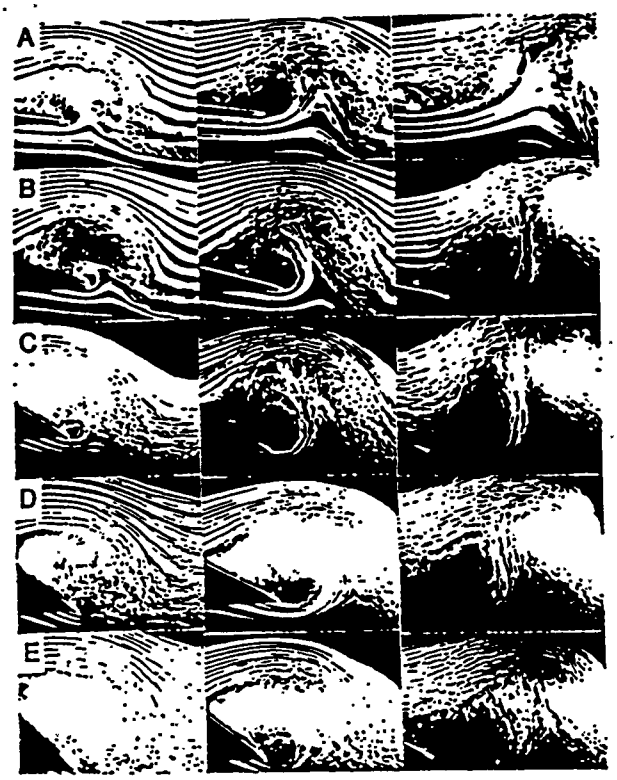

Fig. 1 Trailing edge vortex development behind an oscillating 6" flat plate; Re 40,000, K 0.6, α_ω 6°, osc. axis 0.21; α_m 10,15,20,25,30° A-E.

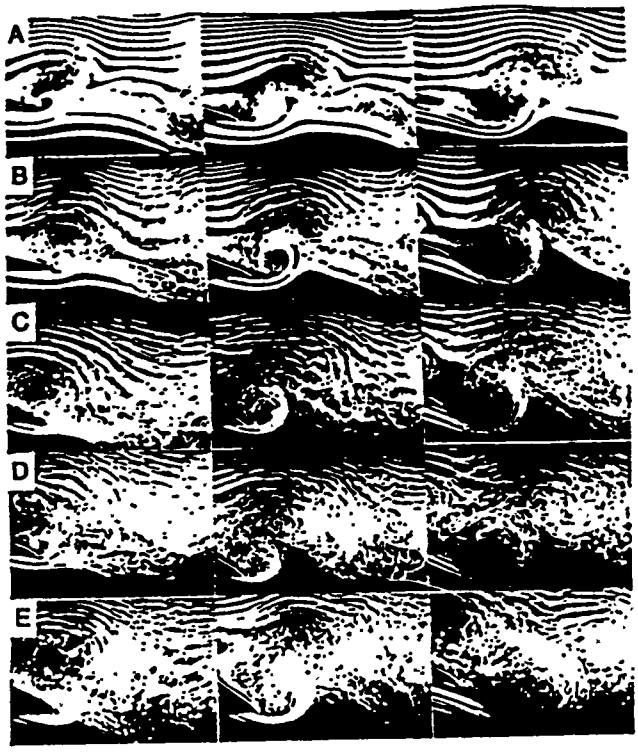

Fig. 2 Trailing edge vortex development behind an oscillating 6" flat plate; Re 26,000, K 1.5, α_ω 6°, osc. axis 0.21c; α_m 10,15,20,25,30° A-E.

attack is shown in column one. With increasing mean angle, the diameter of the leading edge vortex increases to a scale on the order of the chord length. Coupled with the larger vortex size, the smokelines outlining the vortex structure appeared more diffuse. Flow streaklines at the trailing edge also were more diffuse at the larger mean angles.

Complete cataclysmic separation (Fig. 1, column two) occurred coincident with the growth and development of the trailing edge vortex. Separation was highly correlated, visually, with the rapid growth of the trailing edge vortex in the wake. Again, diffuse smoke lines became more prominent in tests using increased angle of attack. Angles of attack of 25° and 30° showed a very diffuse vortex development while lower mean angles (10°, 15°) yielded more cohesive vortex structures.

Approximately one chord downstream of the trailing edge, the vortex interactions in the wake developed into a leading trailing edge tandem vortex structure (Fig.1, column 3). At 15° mean angle of attack (Fig. 1, B; column 3) the leading and trailing edge vortices were fully developed, separated by an upshoot of the smokelines drawn from under the oscillating flat plate. Further increases in mean angle provided minimal change in either the tandem vortex structuring or the coherence of the interactive vortex pair. However, the increases in mean angle appear to position the leading and trailing edge vortices closer together (spatially and temporally) as tandem wake structures.

Reduced Frequency Parameter

As reported earlier, higher rates of pitching produced smaller and decidely more cohesive leading edge vortices. Fig. 2 duplicates the test conditions of Fig. 1 except that the oscillation rate (K = 1.5) is more than twice that shown in Fig. 1. The diameter of the shedding leading edge vortices were significantly smaller at this higher K value (column 1). As above, increasing the mean angle of attack increased the leading edge vortex diameter, however, these diameters were smaller relative to those of the lower K test conditions.

The initiation and interaction of the leading and trailing vortices differed for the two K conditions as well. But, the high K conditions produced cohesive vortices that exhibited a tandem shedding profile that suggested later, mutually disruptive interactions in the wake. The trailing edge vortex initiated as the leading edge vortex approached the trailing edge. The tightly wrapped counter-clockwise circulation of the trailing edge vortex remained more coherent as it shed into the wake. With increasing mean angle, the interaction between the two vortices appeared fully disruptive to the structure of each in the wake. The tandem structuring in the wake appeared both turbulent and diffuse. In sharp contrast, the lower K (K = 0.6) conditions produced more or less simultaneous leading and trailing edge vortex shedding as well as mutually-supported, rapid vertical displacements of the wake. The largest and most cohesive vertical displacements of the wake centered

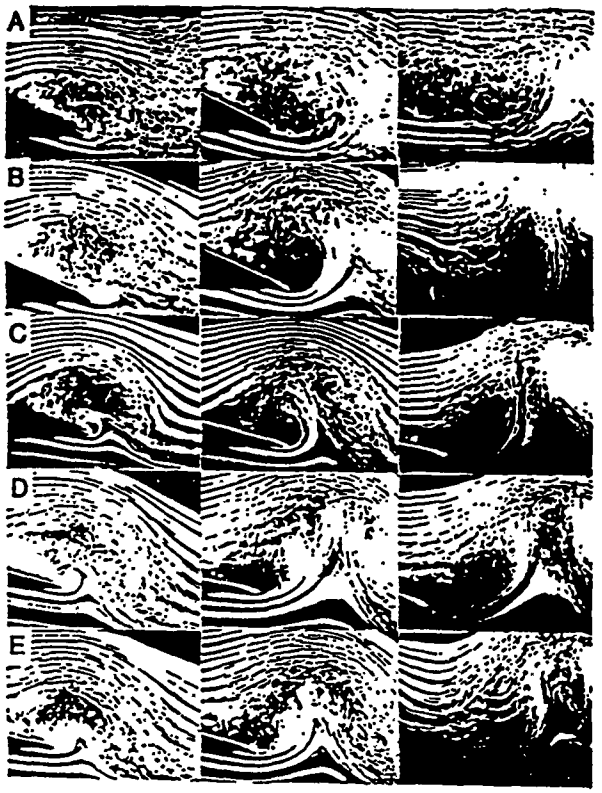

Fig. 3 Trailing edge vortex development behind an oscillating 6" flat plate; Re 40,000, α 15° + 6°, osc. axis 0.21c; K 0.2,0.4,0.6,0.8,1.0 A-E.

around test conditions of K = 0.6 and a mean angle of attack of 20°. Such wake disturbances as characterized by upshoot of the lower smokelines to a position between the tandem vortices were absent in K = 1.5 test conditions regardless of mean angle of attack values examined.

To study the influence of K in more detail (Fig. 3), the wake development was visualized as the reduced frequency parameter values were increased from 0.2 to 1.0 (A-E respectively). Oscillations of the flat plate were driven about a mean angle of 15° with an amplitude of ± 6° for all K values. It is clear that low K values yield the development of a trailing edge vortex just as the leading edge vortex gets to the trailing edge. In contrast, higher K conditions yield formation of the trailing edge vortices only after the leading edge vortices have already begun to shed into the wake. The fully developed flow disturbances in the wake accentuate this difference in that K values greater than 0.2 were associated with the large vertical upshoot component in the wake structure. Cohesion and uniformity in the tandem vortices structure occurs over a limited range of K values. At low K values (0.2), wake structuring appears more turbulent due to overall structure diffusion. Strong reproducibility depended on increasing oscillation frequencies. However, at a reduced frequency of 1.5, the interaction was smaller and more diffuse apparently due to strong disruptive vortex interactions.

Wake Interaction With A Trailing Airfoil

The effects of the vortical wake complex impinging upon a trailing airfoil were investigated using both flow visualization and pressure measures. Fig. 4 depicts the vortical wake created by an oscillating airfoil as this wake impinges upon a trailing airfoil located 0.5 c downstream. Plates A-E show increments in time of 20% through a complete sinusoidal oscillation cycle. Row A photographs were phase-locked to depict the flow interactions as the oscillating airfoil passed through the maximum angle of attack. Columns I, II and III depict flows for three oscillation rates corresponding to reduced frequencies of 0.2, 0.4 and 0.8, respectively. In each of the three columns, the clear Plexiglass mounting support for the trailing airfoil was visible running directly through the center of the pictures. Also, the mounting bolt attaching the airfoil leading edge to the support was outlined by the stroboscopic reflections. The trailing edge of the oscillating airfoil appears to the left of the support and changes position through the oscillation cycle (A-E). Column IV duplicates the test conditions in column III using a different viewing angle. The oscillating airfoil was positioned in the center of the photograph and the leading edge of the trailing airfoil was positioned to the extreme right of the photograph. For all test conditions, the airfoil oscillation dynamics were maintained at a 15° mean angle and ± 6° oscillation amplitude. The trailing airfoil was held at 0° incidence, in line with the pitch axis of the oscillating airfoil.

Previous visualization results had indicated that the most significant alterations in the wake occurred with increasing oscillation rates. To limit the independent parameter range, only the effects of reduced frequency and Reynolds number were examined. Special attention was given the nature of the wake interactions with the trailing airfoil.

Placing a trailing airfoil within the unsteady wake of an upstream oscillating airfoil resulted in only minor changes in the tandem vortex wake development. The strong vertical upshoot between the leading and trailing edge vortices did not appear as pronounced. Vertical displacement of the tandem vortex pair remained evident. The largest change related to the presence of a trailing airfoil could be seen using a reduced frequency of 0.4. Previous results using a single airfoil indicated uniformity in tandem vortex wake development across the same range of reduced frequencies. With a trailing airfoil, however, larger vortex wakes were produced at lower reduced frequencies and more cohesive tandem vortex wakes were produced at higher K values.

The importance of reduced frequency value changes on the temporal aspects of wake vortex development can be discerned readily in Fig. 4. Across row A, the relative position of the leading edge vortex as well as the tandem vortex wake are shown with the oscillating airfoil visualized as it passes through the maximum angle of attack. At a reduced frequency of 0.2 (row A, column one) the tandem vortex wake

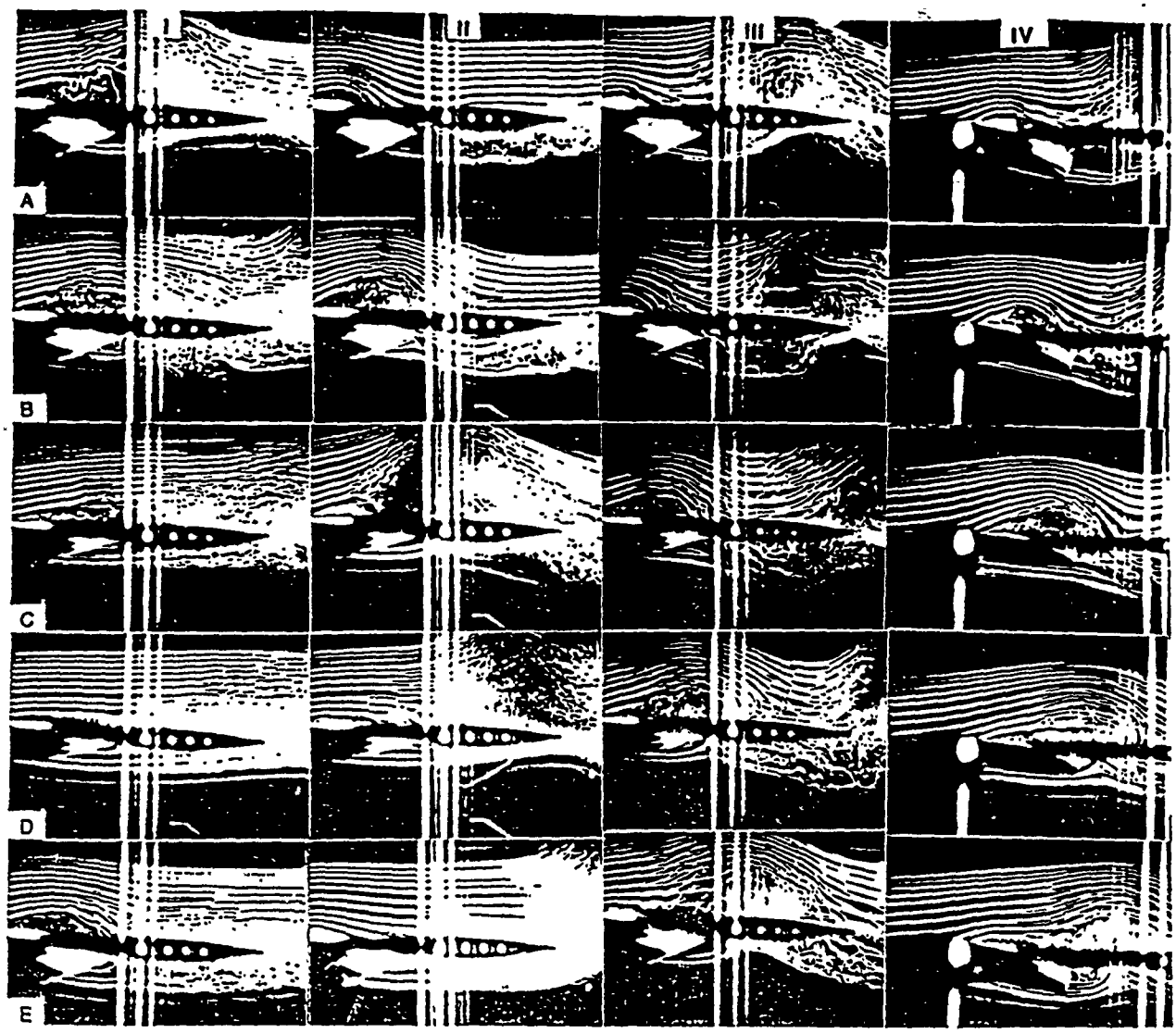

Fig. 4 Vortical wake/trailing airfoil interaction; oscillating airfoil NACA 0015, 6" chord, α 15° ± 6°, osc. axis 0.25c; Trailing airfoil NACA 0015, 6" chord, α 0°, location 0.5c downstream of oscillating airfoil trailing edge; Columns I, II, III K 0.2,0.4,0.8 respectively, column IV K 0.8; Plates A-E 0 (max angle), 20, 40, 60, 80% of the oscillation cycle.

structure was located just over the leading edge of the trailing airfoil. At maximum using K= 0.4 (row A, column two), the leading edge vortex was still located over the oscillating airfoil and no vortical wake structure had formed. At K = 0.8 (row A, column three) the leading edge vortex was only in the initial development stage over the oscillating airfoil. The tandem vortex wake structure visualized over the trailing airfoil had been initiated during the previous oscillation cycle.

Despite the delay in vortex formation, higher K values enhance the wake interaction with the trailing airfoil throughout the pitching cycle. Low K values produce vortices which initiate early in the oscillation cycle and then convect downstream to shed from the airfoil. Large portions of the pitching cycle occur with vortices neither over the pitching airfoil nor in the wake. In contrast, high K values (column three) produce vortices more rapidly, thus reducing the separation distances between successive vortices in the wakes. Vortex wake interactions with the trailing airfoil were more continuous with higher K values.

Previously unreported was the generation of two vortical wakes with each oscillation cycle at low K values. The generation of the second vortex was evident in both the flow visualization and pressure measurements. Column I (K = 0.2) indicated initiation of the leading edge vortex between plates D and E, during the upstroke portion of the oscillation cycle. The wake complex created by shedding of the leading edge vortex convected downstream over the trailing airfoil in plate A and continued farther into the trailing airfoil wake in plate B. Near the leading edge of the trailing airfoil(plate B), a second leading edge vortex appeared. The second vortex was less cohesive and dissipated while convecting over the trailing airfoil. Pressure signatures created by passage of the second vortex will be discussed later.

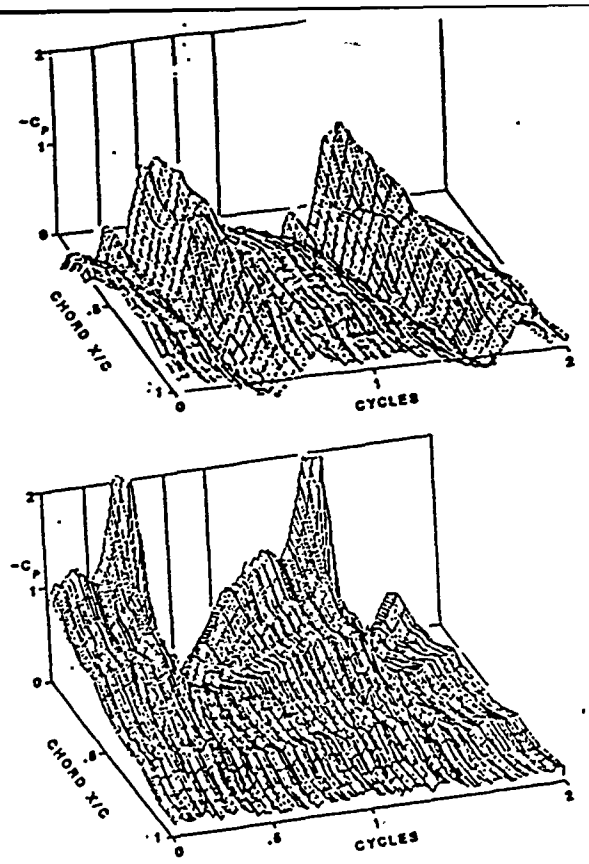

Fig. 5 Unsteady pressure coefficient distributions from vortical wake interactions; Re 50,000, α 0°, top - upper surface, bottom - lower surface; upstream airfoil K 0.4, α 15° + 6°, 0, 1, and 2 cycle locations - airfoil at maximum angle of attack.

Trailing Airfoil-Wake Interaction

Eighteen surface mounted pressure transducers within the trailing airfoil recorded the impact of the tandem vortex wake. Pressure data were collected over two complete oscillation cycles of the upstream airfoil. Twenty five successive runs, phase locked to begin with the oscillating airfoil at maximum angle of attack (t_o), were averaged. Wake structure and wake interaction reliability were measured together with average values. For each test condition, data were collected first on the upper and then on the lower surface in two separate data runs.

Temporally dependent pressure coefficients derived from the pressure measurements were plotted in a three-dimensional topographic fashion showing the magnitude of the pressure coefficient as a function of both chord location and phase of the oscillation cycle (Fig. 5). Three test conditions can be directly compared with the flow visualization results of Fig. 4: Pitching was done at reduced frequencies of 0.2, 0.4 and 0.8 using a freestream velocity of 20 ft/sec. This duplicated the previous flow visualization conditions. The three oscillation rates corresponding to K values of 0.2, 0.4 and 0.8 (periods of 392, 196 and 98 msec, respectively) were then repeated at the higher velocities of 40 and 80 ft/sec. This test matrix permitted examination of wake effects for reduced frequencies of 0.05, 0.1, 0.2, 0.4, 0.8 and Reynolds numbers of 51K, 102K and 204K.

Previous flow visualization results were instrumental to understanding the temporally dependent pressure coefficient results. Fig. 5 shows the change in pressure experienced on both the upper and lower surfaces of the trailing airfoil resulting from interactions with the unsteady wake of the upstream, pitching airfoil. These data were collected at a K value of 0.4 and tunnel speed of 20 ft/sec. Thus, these pressure data correspond to the visualizations in column two of Fig. 4. The four vertical lines in the C_p vs. cycle plot correspond to the plates B, C, D and E, respectively. Plate A, column two, Fig. 4, correlates with the beginnign of each cycle plotted on the pressure coefficient plots (maximum angle of attack).

Many of the perturbations observed in the pressure profiles of Fig. 5 appear across all the test conditions. The upper surface profile was dominated by the presence of a broad large pressure peak occurring midway through each of the oscillation cycles. This large pressure perturbation correlated in time with the visualized passage of the tandem vortex wake complex over the trailing airfoil. For this reduced frequency (K = 0.4), two dominant facets occur within the broad pressure coefficient peak. These identifiable pressure facets appear to represent the passage of the leading then the trailing edge vortex tandem pair over the trailing airfoil.

Prior to the occurrence of the negative pressure coefficient peak associated with the passing wake vortex complex (20% cycle), a small negative pressure peak was observed with two pronounced high pressure valleys on either side. These perturbations appeared to signal the development and approach of the tandem wake process. The first valley formed during the initiation and convection of the leading edge vortex over the upstream airfoil. As the tandem wake developed and approached the leading edge of the trailing airfoil (Fig. 4, column two, B), the induced velocity near the leading edge created a low, brief pressure rise. Impingement of the tandem vortex wake on the downstream airfoil leading edge produced a transient loss in the static pressure rise. This transient reduction was followed by a rapid low pressure rise as the tandem vortex wake fully engaged the trailing airfoil (Fig. 4, column two, B-C; Fig. 5, upper surface, 20-40% cycle).

Similar tandem vortex wake interactions occurred with the trailing airfoil lower surface. The first low pressure rise (Fig. 5, lower surface) had a prominent dip at the 20% phase cycle, correlating with the small pressure rise on the upper surface at the same phase angle of the upstream airfoil. The second, most dominant low pressure peak over the airfoil leading edge, arose during the same portion of the oscillation cycle where the tandem vortices of the wake were convecting over the leading edge of the trailing airfoil. On the upper surface, the low pressure rise persisted over a large portion of the oscillation cycle. This pressure plateau correlated well with the

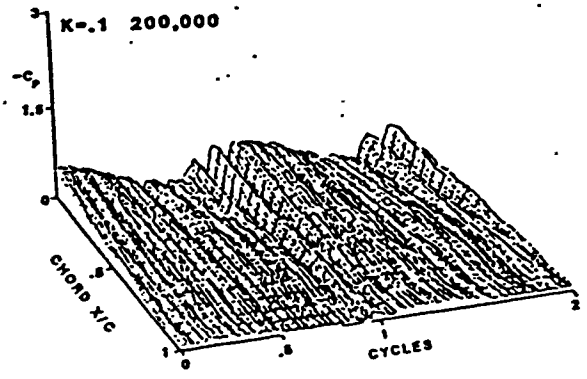

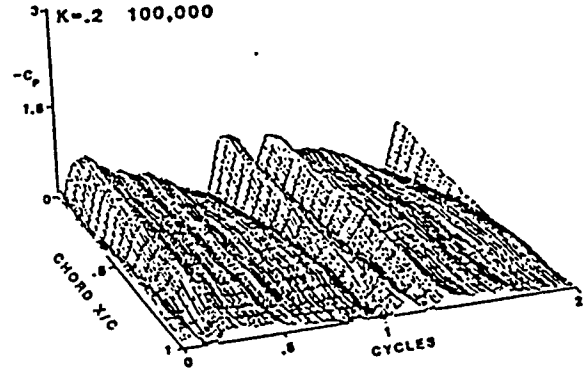

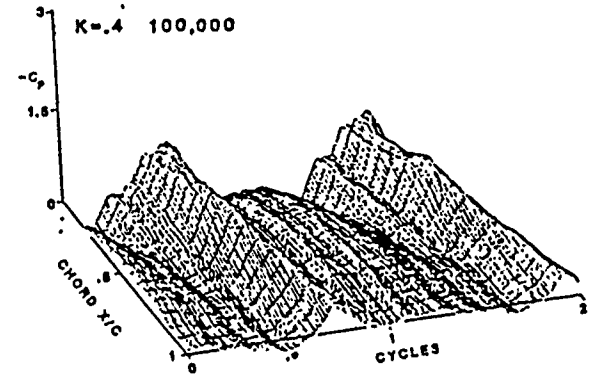

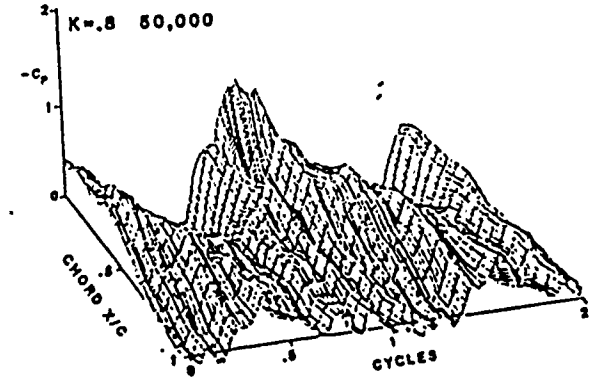

Fig. 6 Reduced frequency effects on the upper surface pressure distributions; α 0°; upstream airfoil α 15° ± 6°, Re 200,100,100, 50K; K 0.1,0.2,0.4,0.8 top to bottom.

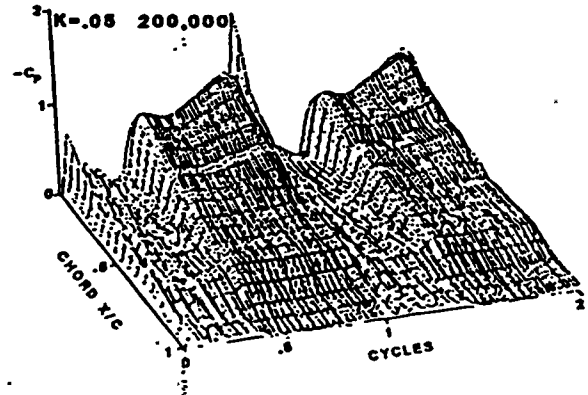

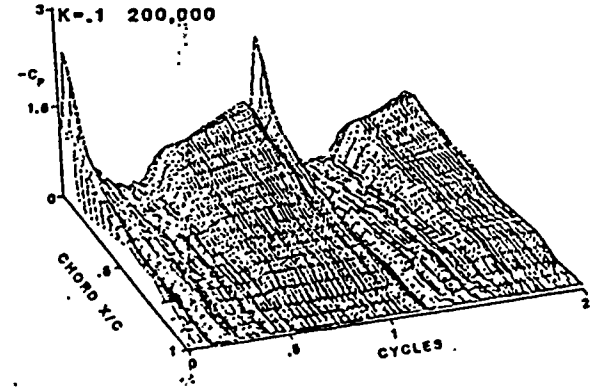

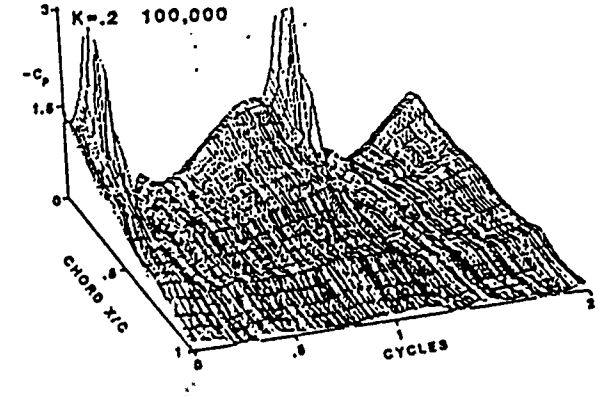

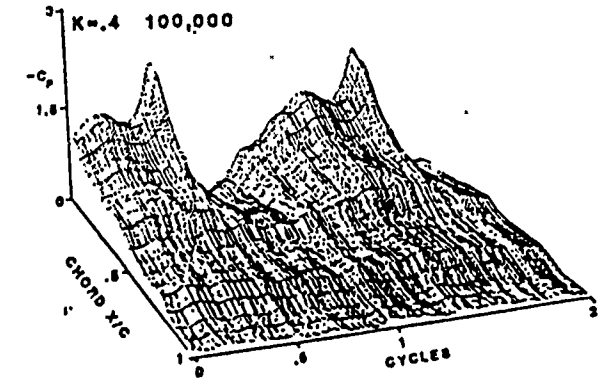

Fig. 7 Reduced frequency effects on the lower surface pressure distributions; 0°; upstream airfoil α 15° ± 6°, Re 200,200,100,100K; K 0.05,0.1,0.2,0.4 top to bottom.

presence of the vortical wake over the trailing, pressure airfoil. In contrast, a rapid pressure rise on the lower surface correlated with the convection of the tandem vortex wake over trailing airfoil surface. This rapid transition from very low to high static pressure occured within 1% of the oscillation cycle and resulted in high static pressure values along the entire chord of the lower surface.

Changes in the reduced frequency directly influenced the intensity, duration and character of the vortical wake interaction with the trailing airfoil. Fig. 6 shows the effects of increased K on the upper surface pressure distributions. At a reduced frequency of 0.1, the pressure signature of only a single vortex is evident just prior to the cycle position of 1.0. Doubling the reduced frequency to K = 0.2, the two separate convecting vortices noted in the visualization data were also evident in the pressure profiles. The initiation of the first occurred on the upstroke prior to maximum angle of attack in the pitching cycle, while the second occurred on the downstroke and was convecting at 25% of the pitching cycle. Further pitching increases to K = 0.4 initiated the presence of a single vortex. The passage of this vortex over the trailing airfoil had a greater pressure influence than observed with the two vortices of K = 0.2. The pressure plateau shown midway through the overall pressure rise signaled the advent of vortex impingement on the trailing airfoil. At a reduced frequency of 0.8, the peak value of the pressure rise over the leading edge remained relatively constant. The planar cut through the pressure profile curve at t_o (0 cycle) shows the residual influence exerted by the convecting tandem vortex wake initiated in the previous oscillation cycle. Flow visualization results in Fig. 4, column three, row A show the location of the tandem vortex wake over the trailing airfoil.

Increase in the reduced frequency changed the phase and duration of the vortical wake influence on the trailing airfoil. These phase shifts were most apparent in the phases of the pitching cycle associated with vortex impingement on the trailing airfoil. Low K rates (K > 0.2) indicated the beginning of wake/airfoil interactions prior to the leading airfoil reaching maximum angle of attack (t_o). Larger oscillation rates (K values) delayed these interactions to later portions of the leading airfoil oscillation cycle. Also, as noted earlier in the visualization results, some portion of the tandem vortex wake resided over the trailing airfoil for increasing percentages of the oscillation cycle with increasing K values.

These same trends in phase shift at higher K values existed for the lower surface pressure profiles as well. Increasing oscillation rates shifted the dominant peak in the lower surface profile to later phases of the oscillation cycle. Duration of the pressure rise on the lower surface, however, was not a direct reflection of the oscillation rate. Lower K (0.05) rates generated a negative pressure coefficient rise as the leading airfoil began to pitch from the minimum to the maximum angle of attack (0.5 cycle). This pressure rise culminated in a distinct sharp pressure peak near the leading edge indicating impingement of the vortex wake complex on the trailing airfoil. After the tandem vortex wake passed over the leading edge, a pressure rise occurred rapidly and remained until the leading airfoil returned to the minimum angle of attack. The low pressure coefficient rise, peak and transition to high pressure remained the dominant characteristics of the lower surface pressure fluctuations across all K values. Initiation of the low pressure coefficient rise always occurred at 0.5 cycle for K = 0.2. At K = 0.4, delay in the impingement of the vortex wake to 0.5 cycle preempted the low pressure rise with a dominate low pressure peak.

Pressure distributions on the upper and lower surface also varied with Reynolds number. In Fig. 8, Reynolds numbers of 50,000 and 100,000 show the double tandem wake formation discussed previously for K values of 0.2. At 200,000, the pressure coefficient profiles returned to the single tandem vortex wake structure observed with larger oscillation rates. Impingement delays to later phases of the cycle were evident also. Increasing Re also delayed pressure peak signatures from the wake impingement on the leading edge to later portions of the oscillation cycle. Similarly, Reynolds number effects for reduced frequencies of 0.1 and 0.4 included delays in cycle phase with increasing Re. Most importantly, alterations in the pressure profile shapes did not occur with Re variations.

The largest pressure peaks on both the upper and lower surface were elicited when the tandem vortex wake impinged upon the leading edge of the trailing airfoils. On the upper surface the pressure maxima were greatest at the leading edge and diminished gradually as the vortex wake convected over the airfoil. The lower surface exhibited a brief low pressure rise characterized by a sharp peak. This rapidly transitioned to a high pressure along the lower surface chord. The maximum peak pressure deficit affected only the first 0.25c of the airfoil. The magnitudes of these low pressure peaks as a function of Reynolds number and reduced frequency are plotted in Fig. 9. On the average, peak low pressures were two to three times greater on the lower surface than on the top surface; the largest negative peaks occurring at K = 0.2. On the upper surface the peak low pressure coefficients increased in linear fashion with increasing K. In contrast, low pressure peaks on the lower surface initially increased with oscillation rate (K< 0.2) and then diminished at larger reduced frequencies. Differences in Reynolds number produced only minor variations in these pressure peaks.

Figs. 10 and 11 highlight the effects of reduced frequency and Reynolds number on the lift coefficient generated by the trailing airfoil. Integration of the previous pressure profiles generated the temporally-dependent lift coefficients over two oscillation cycles of the leading airfoil. Across test conditions, the lift coefficient plots showed prominent transitions from negative to positive peak

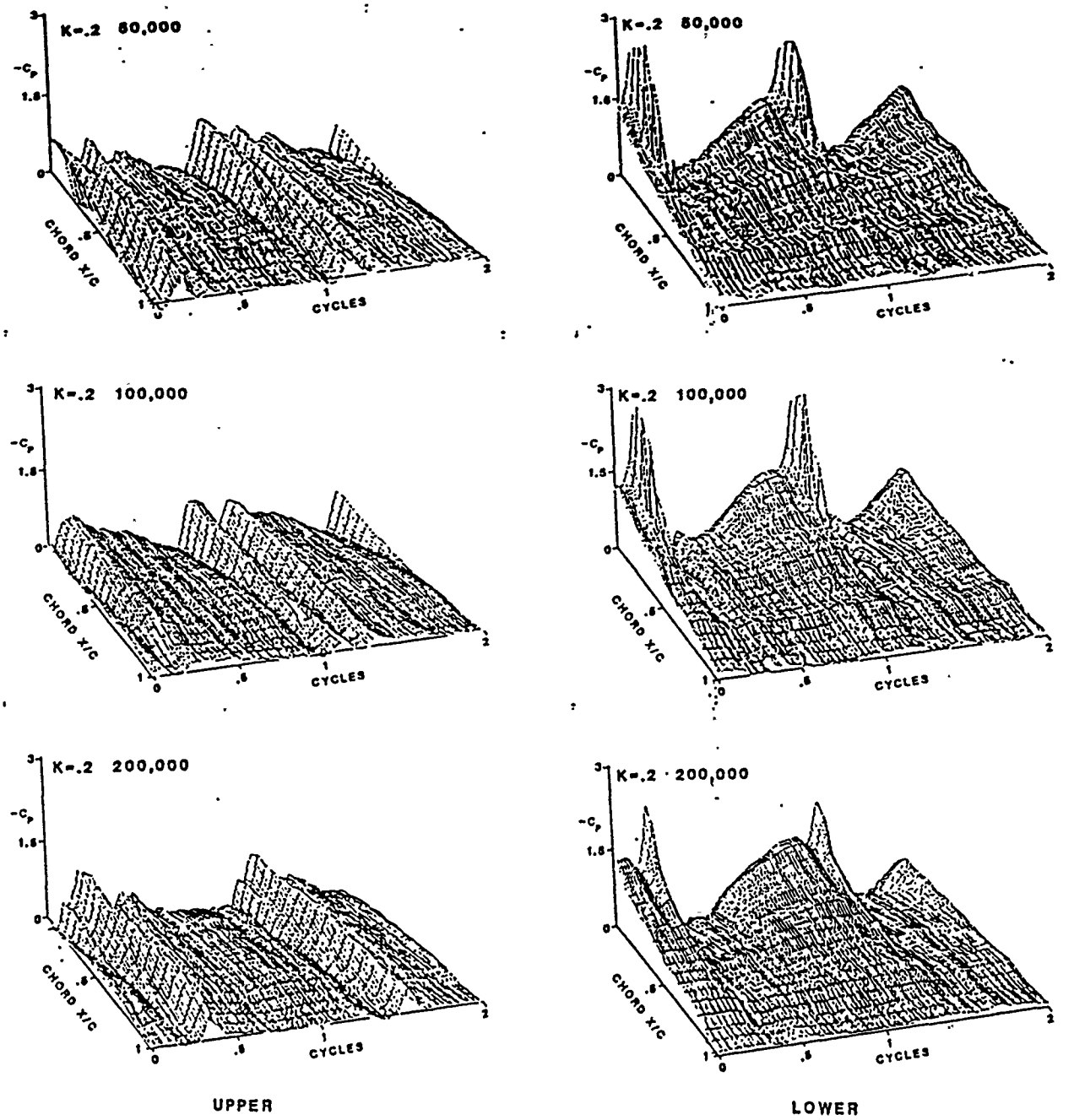

Fig. 8 Reynolds number effects on the upper and lower surface pressure distributions; α 0°; upstream airfoil α15° $\pm$ 6°, K 0.2; Re 50,100,200K top to bottom.

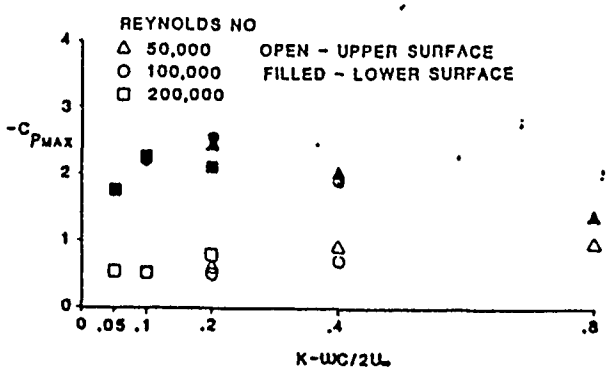

Fig. 9 Maximum pressure peaks induced by airfoil/wake interactions.

values during the oscillation cycle. These transitions can be correlated with specific events in the pressure profiles. The onset of lift value sign transitions developed when the low pressure peaks on the bottom airfoil surface rapidly changed to a high pressure region along the whole chord. The low pressure produced on the upper surface by the passing vortex wake generated the net positive lift.

Not surprisingly, many of the previously reported effects of reduced frequency and Reynolds number on the pressure profiles were reflected in the C_L plots (Fig. 10). Increasing the reduced frequency delayed the C_L transition peaks in the oscillation cycle. The repeatability of C_L, cycle to cycle, was

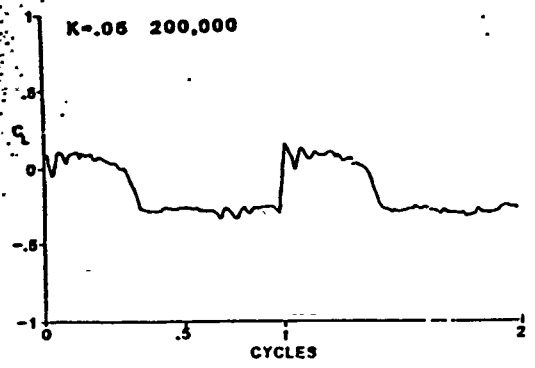

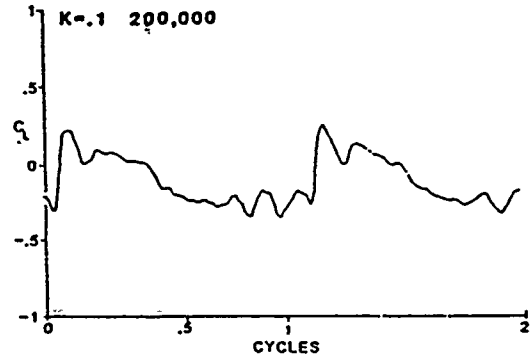

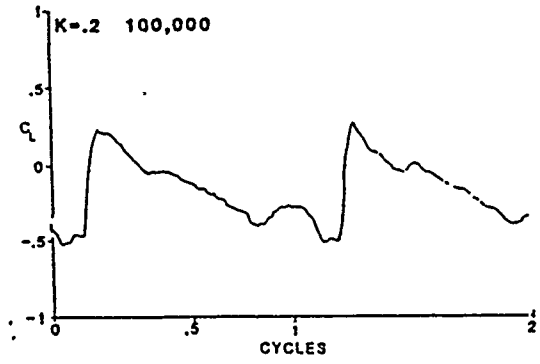

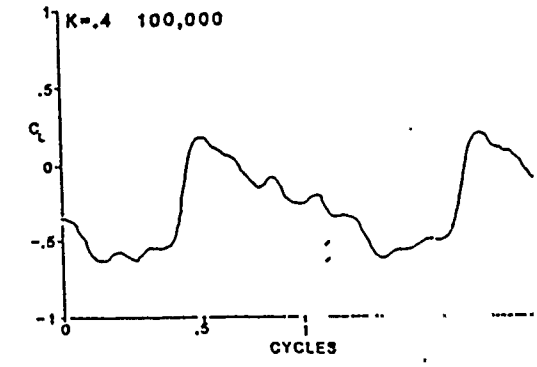

Fig. 10 Reduced frequency effects on the unsteady lift coefficients; α 0°; upstream airfoil α 15° ± 6°, Re 200,200,100,100K; K 0.05,0.1,0.2,0.4 top to bottom.

indicative of the reproducibility in unsteady pressure profiles generated by the vortex wake interactions. Likewise, Reynolds number effects (Fig. 11) yielded both the expected phase shift consequences and the characteristic flow reproducibility. Differences in the shape of the C_L curves with increasing Reynolds number demonstrated the temporal sensitivity of wake

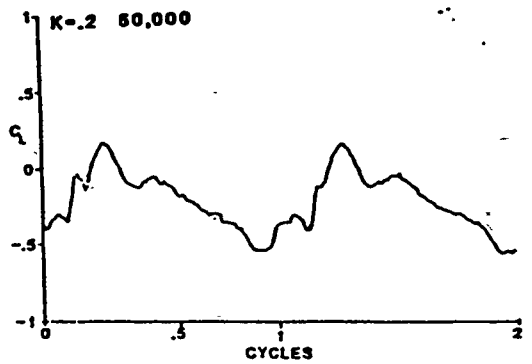

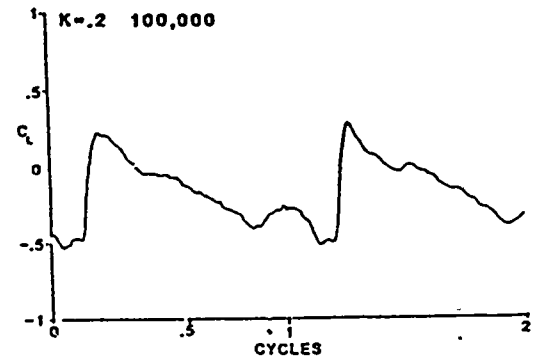

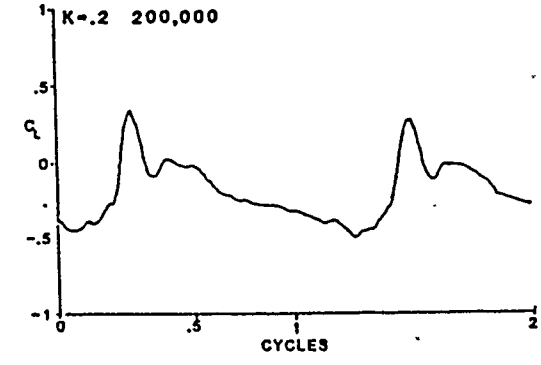

Fig. 11 Reynolds number effects on the unsteady lift coefficients; α 0°; upstream airfoil α 15° ± 6°, K 0.2, Re 50,100,200K top to bottom.

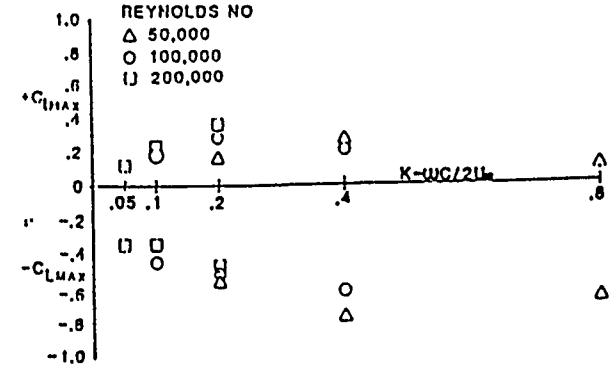

Fig. 12 Maximum C_L transients induced by airfoil/wake interactions.

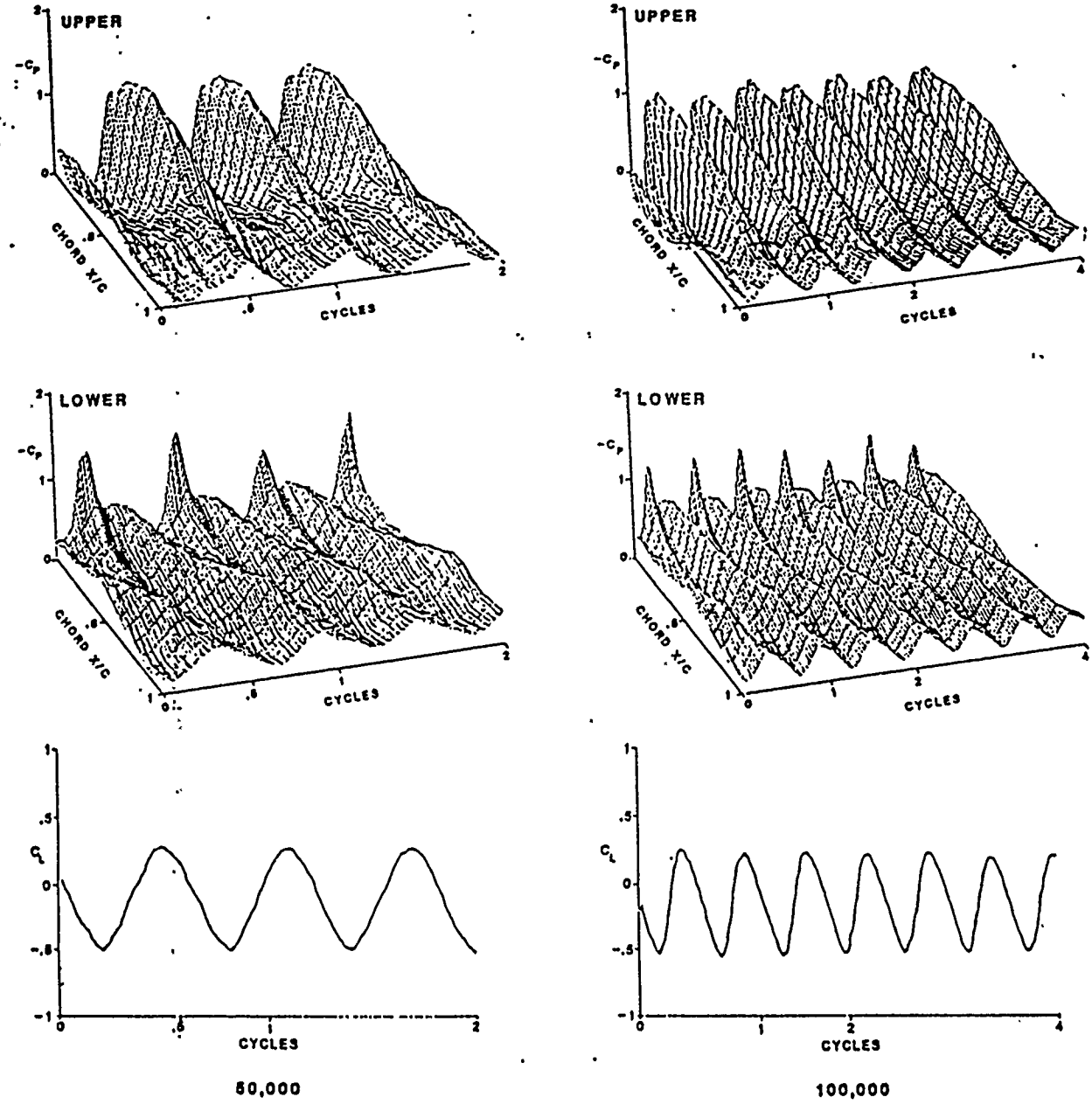

Fig. 13 Unsteady pressure and lift coefficients produced by an auto-rotating flat plate 0.5c upstream of a stationary airfoil at 0°; 3" flat plate, left - Re 50,000, right - Re 100,000; effective reduced frequency 1.6 and 1.8 for Reynolds numbers of 50 and 100 K.

development to changes in independent test variable.

The maximum and minimum C_L values obtained over the oscillation cycle were plotted as a function of Reynolds number and reduced frequency in Fig. 12. Corresponding to the low pressure values on the lower surface, the negative peak C_L' amplitudes were larger than the corresponding positive values. Both positive and negative values increased with oscillation rate for $K < 0.1$. Larger reduced frequencies ($0.2 \leq K \leq 0.8$) decreased the peak positive values but the negative values continued to increase at $K = 0.4$. Between $0.4 \leq K \leq 0.8$ the peak negative C_L remained constant at -0.6. Note that these transitions in C_L from negative to positive values range in magnitude from 0.4 to 1.0 and transition within a few percent of the total oscillation cycle.

For comparison, the unsteady wake effects produced by an auto-rotating flat plate were plotted in Fig. 13. The left column documents the effects at 20 ft/sec while the right shows unsteady pressure and lift coefficients at 40 ft/sec. Unlike an oscillating airfoil, two wakes are created with each complete rotation cycle of the 3" flat plate. The effective reduced frequencies based upon the half-cycle rotation of the flat plate were $K = 1.8$ and 1.6 for 20 and 40 ft/sec, respectively. Vortices produced from auto-rotation of a flat plate shed from both the upper and lower edges as the plate approached a vertical orientation. Passage of these two vortices over the trailing airfoil were recorded in the pressure data. The large pressure rise on the upper surface correlated

with the sharp pressure spike on the lower surface profiles and indicated passage of the upper surface vortex initiated from the retreating edge of the flat plate. Unlike the oscillating airfoil wake, the vortex initiated from the advancing edge of the rotating plate passed beneath the trailing airfoil. On the lower surface, the maximum pressure peak was followed by the low pressure rise created by this passing vortex beneath the airfoil. Maximum $-C_p$ values produced on the upper and lower surfaces were 1.0 and 1.2 respectively, duplicating the pressure peaks obtained for an oscillating airfoil at K = 0.8. Also, maximum and minimum values of C_L peaked at +0.25 and -0.5, values very close to the magnitudes of 0.1 and 0.7 at K = 0.8 for the oscillating airfoil. The mean C_L values between peaks for the two different test conditions were 0.75 and 0.8, respectively.

Discussion

Sinusoidal oscillations of an airfoil or flat plate beyond static stall produced reproducible unsteady vortex dominated wakes. The wake structure consists of two vortex components initiated during the sinusoidal oscillation cycle. These vortices combined in the wake to form a tandem vortex complex. The first vortex, leading the combined pair, originated from the forced unsteady flow separation at the airfoil leading edge and usually occurred during the upward pitching portion of the cycle. Shedding of the separation induced vortex from the trailing edge of the oscillating airfoil initiated the second or trailing edge vortex. Rapid growth of both vortices ensued in the wake. One chord downstream of the oscillating airfoil, the vortex dominated wake was fully developed and appeared as a tandem vortex pair separated by a vertical flow upshoot between the two vortices.

Alterations in the airfoil motion history directly influenced the size, shape and shedding phase angle of the vortices in the wake. Parameters governing the airfoil motion history previously have been observed to bias the initiation and development of both the leading and trailing edge vortices. Not surprisingly, the same parameters affected the wake development in much the same way. Increased oscillation rate delayed vortex initiation to later periods in the oscillation cycle. This delayed initiation was reflected in delayed development of the vortical wake as well.

Rapid oscillation rates decreased the separation distance between successive leading edge vortices. With a tandem vortex wake structure being produced for each oscillation cycle, multiple tandem vortex wake structures were evident in the flow field with high K values. This rapid, continuous production of successively generated tandem structures resulted in nearly continuous trailing airfoil/vortex interactions.

Reduced frequency had previously been observed to play an important role in the size and cohesion of leading edge vortex structures. Vortices produced over the oscillating airfoil at high oscillation rates were small and tightly bound into cohesive structures. The effects of oscillation rate on the tandem vortex wake development were more complicated. Over a narrow range of K values, increases enhanced the tandem wake cohesion. At high K values ($K \geq 1.5$), where the vortices were simultaneously present at the airfoil trailing edge, the vortex-vortex interactions appeared mutually disruptive. At reduced frequencies between $0.2 \leq K \leq 0.8$, very little alteration was present in the fully developed tandem wake vortex.

Changes in mean angle of attack also played an important role in the tandem vortex wake development. In general, greater mean angles produced larger leading edge vortices. These larger vortices exhibited less smokeline cohesion. But, this effect did not carry over to the tandem wake vortex development. Wake cohesion, shape and size were affected only at the extremes of the parametric range $10° < \alpha < 30°$. Between these limits, the fully developed tandem vortex wake was insensitive to mean angle of attack variations. Angles below 10° initiated smaller, more cohesive wakes while large angles ($\alpha > 30°$) resulted in more disparate wake development.

The presence of a trailing airfoil in the wake did produce two notable changes in the tandem vortex wake development. Wake development behind a single pitching airfoil possessed notable vertical flow upshoot between the tandem vortices of the wake. This flow perturbation was disrupted by the presence of the trailing airfoil. Also characteristic of the presence of a trailing airfoil were larger vortices exhibiting greater vertical displacements, especially evident at low K values. Over the same parameter range, the wake of a single airfoil had indicated uniformity in tandem vortex structure development. The second modification produced by the trailing airfoil was the development of two tandem vortex wake structures with each oscillation cycle using K = 0.2. The second structure was evident in both the visualization and pressure results. Previous visualization results for the same test conditions failed to show double vortex initiation. However, experiments by Helin et al.[10] had noted the generation of a second leading edge vortex generation when large, single pitch airfoil motions at constant rotation rates were used.

Vortical wake impingement on a trailing airfoil resulted in severe transient loading on the trailing airfoil created by the low static pressure rise on the upper airfoil surface. The magnitude, duration and cycle phase of these loads were dependent upon the rate of oscillation and Reynolds number. Earlier investigations of vortex development over the oscillating airfoil noted dominant, spatially localized low pressure peaks produced by the leading edge vortex. The translation of the vortex over the chord was easily discerned by simply tracking the pressure peak that convected along the chord as indicated in the pressure profiles.

Vortical wake interactions had a much more global pressure effect. The diameter of the

tandem vortex structure was on the same order as that of the trailing airfoil chord. Thus, low pressure influences created by the passing wake complex covered large portions of the trailing airfoil chord and exhibited more broad, spatially diffuse pressure effects. Across test conditions, however, peak low pressure influences were greatest at the leading edge and dissipated with the convection and growth of tandem wake structure over the trailing airfoil.

Earlier experiments noted a pronounced effect on transient peak pressure coefficients and subsequent lift values when high oscillation rates (increased K values) of an oscillating airfoil were employed. These results do not carry over in a simple way to the wake interactions that occur on a trailing airfoil. Peak low static pressures exerted on the upper surface of the trailing airfoil by the passing wake indicate moderate changes in $-C_p$ peaks from 0.5 to 1.0 with a reduced frequency change from flat plate are included, the $-C_p$ stays the same and the K range extends to 1.8.

Unsteady lift values on the trailing airfoil actually diminish with increasing K. The positive peak values of lift coefficient average approximately +0.2 across all Reynolds numbers and reduced frequencies. The positive peak lift coefficient decreases with increasing K from $0.2 < K \leq 1.8$. In contrast, the negative peak lift coefficients were enhanced from -0.3 to -0.7 over the same K range. Though actual integrations of the C_L vs. cycle curves were not performed, a cursory examination indicates that an overall negative lift averaged over the oscillation cycle would be obtained on the trailing airfoil for all test conditions.

The overall net negative lift was largly the result of the unsteady pressure effects produced by the oscillating airfoil on the lower surface of the trailing airfoil. The unsteady low pressure rise on the lower surface was comprised of two separate unsteady events: 1) a gradual uniform rise in low static pressure along the chord at 0.5 cycle and 2) a transient peak near the leading edge correlated with the passing vortex wake. Though the transient peak created the largest pressure influence, the gradual low pressure rise at 0.5 cycle sustained over large portions of the oscillation cycles and appeared to be responsible for the overall negative lift through the cycle.

The gradual pressure rise at 0.5 cycle possessed the characteristics of auniform flow along the trailing airfoil lower surface. One possible explanation for this effect may be the reattachment of flow over the oscillating airfoil. At 0.5 cycle the oscillating airfoil reversed direction from downstroke to upstroke at the minimum angle of attack. During the upstroke portion of the pitching cycle, it is well documented that the separated flow over the oscillating airfoil dynamically reattaches and follows the airfoil contour. The dynamically attached flow leaves the oscillating airfoil trailing edge tangent to the local angle of attack. For these experiments, the trailing airfoil was located 0.5c downstream and at the same height as the oscillating airfoils pitch axis. Flow leaving the oscillating airfoil trailing edge, thus, would be channeled around the trailing airfoil lower surface. The flow direction would appear as a negative angle of attack relative to the trailing airfoil. This negative angle would increase as the oscillating airfoil pitched toward maximum angle of attack. The overall result would be an increase in low static pressure about the airfoil lower surface and an increasing negative lift shown throughout the cycle. Changes in the position of the trailing airfoil relative to the oscillating airfoil could radically change the resultant pressure distributions. Ideally, the position of the trailing airfoil could be changed as the oscillating airfoil pitches through the oscillation cycle.

Another potential control problem would be caused by the dependence of the pressure magnitudes and resultant lift coefficients on Reynolds number. Previous unsteady pressure and lift coefficient results from different airfoils driven sinusoidally and with constant pitch motions were Reynolds number independent. The reduced frequency parameter or non-dimensional pitch rate provided an adequate parameter to predict the unsteady effects. The present results show both phase shifts and variances in wake development related to Reynolds number changes. Further investigations examining both relative trailing airfoil placement and larger Reynolds number ranges at different fixed reduced frequencies should help to explain the Reynolds number dependence suggested by the present studies.

Conclusions

It appears clear that a reproducible, phase-dependent, tandem vortex wake was the byproduct of forced unsteady separated flow generated by a sinusoidally oscillating airfoil. The tandem structure was comprised of the combined leading and trailing edge vortices as they shed from the oscillating airfoil. Changes in the dynamic parameters that affected the airfoil motion history produced only minor alterations in the fully developed wake structure. Only at the extreme limits of reduced frequency ($K \leq 0.1$, $K \geq 1.5$) and mean angle of attack ($\alpha_m \leq 10°$, $\alpha_m \geq 30°$) did significant changes in wake structure size and cohesiveness occur. Unlike the intensive, cohesive leading edge vortex produced over the oscillating airfoil at large K values, the tandem vortex wake appeared more diffuse and interactively disrupted especially with increasing angle of attack.

Pressure distributions over the trailing airfoil were significantly altered by the passing wake and large load transients were in evidence. Convection of the vortical wake over the upper surface was easily tracked in the pressure profiles. Lower surface pressure distributions revealed a broad continuous signature characteristic of uniform flow attachment. These signatures were abruptly terminated with a localized peak of rapid transition to high pressure about the chord. This continuity of pressure flux across test conditions was attributed to three separate events in the airfoil oscillation cycle: 1)

dynamic attachment of the flow over the oscillating airfoil directing flow downward and under the lower airfoil surface, 2) passage of the wake complex over the upper leading edge and 3) disruption of flow about the lower surface during passage of the wake complex. The rapid transition from low to high static pressure on the lower surface, coupled with the low static pressure created by passage of the vortical wake over the upper surface, resulted in the large negative to positive lift coefficient transients in all of the C_L data. Over the range of reduced frequencies tested, increasing K values produced little change in either the peak pressure magnitudes or the overall transient lift characteristics. However, increased oscillation rates did alter both the phase and angles of the wake/airfoil interactions throughout the oscillation cycle.

It is apparent that the vortical wake produced behind an airfoil oscillating beyond static stall may produce serious, adverse effects when impinging upon trailing bodies. Though both reproducible and predictable, the magnitudes and short duration transient behaviors offer significant control problems. Further investigations incorporating different airfoil motions and trailing airfoil locations as independent parameters are warranted to define the potential adverse effects of these interactions and to identify means for avoiding them.

Acknowledgments

The authors greatly appreciate the support of Major John Walker and the Seiler Research Laboratory for the data reduction of the unsteady pressure measurements. This work has been sponsored by the U. S. Air Force Office of Scientific Research, grant number AF-F49620-84-C-0065. The technical assistance of W. Bank and R. Meinzer was appreciated. Manuscript prepared by J. Button and S. Walts.

Bibliography

1. McCroskey, W.J., "Some Current Research in Unsteady Fluid Dynamics - The 1976 Freeman Scholar Lecture," J. Fluids Engineering, vol. 99, pp. 8-38, 1977.

2. McCroskey, W.J., "Unsteady Airfoils," Annual Review Of Fluid Mechanics, pp. 285-311, 1982.

3. Reynolds, W.C. and Carr, L.W., "Review of Unsteady, Driven, Separated Flows," AIAA Paper 85-0527, 1985.

4. Favier, D., Maresca, C. and Rebent, J., "Dynamic Stall Due to Fluctuations of Velocity and Incidence," AIAA Paper 81-1288R, 1981.

5. Ham, N.D., "Aerodynamic Loading on a Two-Dimensional Airfoil during Dynamic Stall," AIAA Journal, Vol. 6, pp. 1927-1934, 1968.

6. Johnson, W., "The Effect of Dynamic Stall on the Response and Airloading of Helicopter Rotor Blades," J. American Helicopter Society, Vol. 14, pp. 68-79, 1969.

7. Robinson, M.C. and Luttges, M.W., "Vortex Generation Induced by Oscillating Airfoils: Maximizing Flow Attachment," 8th Biennial Symposium on Turbulence, Rolla, MO., pp. 13.1 - 13.10, Sept. 1983.

8. Robinson, M.C. and Luttges, M.W., "Vortices Produced by Pulsed Air Injection from the Surface of an Oscillating Airfoil," AIAA Paper 86-0118, 1986.

9. Luttges, M.W., Robinson, M.C. and Kennedy, D.A., "Control of Unsteady Separated Flow Structures on Airfoils," AIAA Paper 85-0531, 1985.

10. Helin, H.E., Robinson, M.C. and Luttges, M.W., "Visualization of Dynamic Stall Controlled by Large Amplitude Interrupted Pitching Motions," AIAA Paper 86-2281 CP, 1986.

11. Herbst, W.B., "Supermaneuverability," Joint Automatic Control Conference, Univ. of VA, Jun 17-19, 1981; See also Workshop in Unsteady Separated Flow, USAF Academy, Aug. 1983, published by the University of Colorado, Department of Aerospace Engineering.

12. Commerford, G.L. and Carta, F.O., "An Exploratory Investigation of the Unsteady Aerodynamic Response of a Two-Dimensional Airfoil at High Reduced Frequency," AIAA Paper 73-309, 1973.

13. Sears, W.R., "Some Aspects of Non-Stationary Airfoil Theory and its Practical Application," J. Aeronautical Science, Vol. 8, pp. 104-108, 1941.

14. Kovasznay, L.S.G. and Fujita, H., "Unsteady Boundary Layer and Wake Near the Trailing Edge of a Flat Plate," Proc. IUTAM Symposium at Laval, Canada, p. 805, 1972.

15. Ho, C.M. and Chen, S.H., "Unsteady Wake of a Plunging Airfoil," AIAA Paper 80-1446, 1980.

16. Telionis, D.P., and Poling, D.R., "The Response of Airfoils to Periodic Disturbances--The Unsteady Kutta Condition," AIAA Paper 84-0050, 1984.

17. Walker, J.M., Helin, H.E., and Chou, D.C., "Unsteady Suface Pressure Measurements On a Pitching Airfoil," AIAA Paper 85-0532, 1985.